International Journal of Pharmaceutics: X 8 (2024) 100301

Contents lists available at ScienceDirect

International Journal of Pharmaceutics: X

journal homepage: www.sciencedirect.com/journal/international-journal-of-pharmaceutics-x

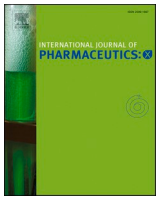

Olive mill wastewater: From by-product to smart antioxidant material

Marco Ruggeri [a], Fabrizio De Luca [b], Amedeo Ungolo [a], Barbara Vigani [a], Alejandro J. Paredes [c], Eleonora Russo [d], Maria Grazia Bottone [b], Eleonora Bianchi [a], Franca Ferrari [a], Silvia Rossi [a], Giuseppina Sandri [a,*]

[a] Department of Drug Sciences, University of Pavia, 27100 Pavia, Italy
[b] Department of Biology and Biotechnology "L. Spallanzani", University of Pavia, 27100 Pavia, Italy
[c] School of Pharmacy, Queen's University Belfast, Medical Biology Centre, Belfast, United Kingdom
[d] Department of Pharmacy, University of Genoa, 16132 Genoa, Italy

ARTICLE INFO

Keywords:
Wound healing
Olive mill wastewater
Gene expression
Oxidative stress

ABSTRACT

Olive mill wastewater (OMWW) is a byproduct of olive oil extraction that represents a critical environmental concern due to its potential adverse effects on ecosystems. Given these premises, spray-dried microparticles were designed and developed using maltodextrins as carriers to encapsulate OMWW bioactive compounds. The microparticles were manufactured using an easily scalable and sustainable spray-drying process. The resulting microparticles were smooth, spherical, and exhibited a mean particle size of about 18 μm. The systems demonstrated notable antioxidant properties with a DPPH radical scavenging activity higher than 60 %, due to the polyphenolic compounds of OMWW (about 24 g gallic acid equivalents per g of sample). In addition, the microparticles supported fibroblast and macrophage viability at concentrations up to 1 mg/mL. They also determined a 4-fold inflammation reduction in macrophages, improved collagen expression in fibroblasts, and modulated oxidative stress on aged fibroblasts. In conclusion, these microparticles could be considered as promising medical devices in wound healing, while offering a sustainable solution for valorizing OMWW.

1. Introduction

Extra virgin olive oil (EVO) is a cornerstone of the Mediterranean diet and culture, celebrated worldwide for its flavor and health benefits (Bilal et al., 2021). The process of producing EVO generates three main residual products: olive pomace, twigs and leaves, and olive mill wastewater (OMWW). OMWW is a dark red to black liquid with high conductivity and mild acidity (Al-Qodah et al., 2022). It comprises water (83–92 % *w*/w), sugars, fermentable proteins, organic acids (such as acetic, fumaric, glyceric, and oxalic acids), small amounts of emulsified olive oil, phenols, waxy and resinous substances, and vitamins. Phenols in OMWW are mainly present as glucosides, tannins, anthocyanins, and lignin. The amount of OMWW produced varies significantly based on factors like the efficiency of extraction methods, and the quality of the olives processed (Shabir et al., 2023). On average, processing one ton of olives generates 500–1100 l of OMWW (Moglie et al., 2024) and this necessitates robust management strategies to address its environmental impact. In addition, OMWW exists in two distinct types depending on the processing method. In the continuous three-phase process, OMWW is highly diluted but rich in polyphenols because it uses a great amount of water, which extracts these bioactive compounds. On the other hand, OMWW from the traditional discontinuous process is more concentrated, with a lower content of polyphenols due to the use of less water (Aggoun et al., 2016). These differences have marked implications for environmental management and potential recovery of polyphenols.

OMWW poses significant environmental concerns. Despite being biodegradable, it threatens aquatic life by reducing oxygen availability, increasing eutrophication, and changing water colour. Its acidic pH and phenol content make it phytotoxic, and it ferments, causing odor pollution. Additionally, its lipid content can form films that lead to plant overgrowth (Alkhalidi et al., 2023; Sciubba et al., 2020).

Sustainable solutions are being evaluated to reduce the environmental impact of OMWW, mitigating these risks by reusing or recycling it with various efforts (Carmona et al., 2023). OMWW can be transformed into various carbonaceous materials, such as biochar and activated carbon, through advanced treatments, offering a beneficial solution to reduce environmental impact and contribute to the circular economy for OMWW (Mechnou et al., 2023; Mechnou et al., 2024).

* Corresponding author.
E-mail address: g.sandri@unipv.it (G. Sandri).

https://doi.org/10.1016/j.ijpx.2024.100301
Received 31 July 2024; Received in revised form 5 November 2024; Accepted 5 November 2024
Available online 7 November 2024
2590-1567/© 2024 The Authors. Published by Elsevier B.V. This is an open access article under the CC BY-NC-ND license (http://creativecommons.org/licenses/by-nc-nd/4.0/).

Some studies reported the use of OMWW as fuel in thermochemical treatment for heat and electrical energy production (Christoforou and Fokaides, 2016), while others include biotransformation techniques, such as composting or the extraction of value-added phytochemical compounds like phenolic compounds (Tortosa et al., 2012; Nunes et al., 2018). However, these applications led to limited success as such techniques for OMWW conversion were economically unfeasible or inappropriate for large-scale industrial production, limiting their impact.

Given these premises, this work was focused on valorizing and recycling OMWW through a sustainable and scalable process to create a high-value medical device for wound healing within a circular economy framework. In particular, OMWW was transformed from waste into a valuable source of material by developing spray-dried microparticles using maltodextrin as a carrier to encapsulate OMWW bioactive compounds. The microparticles were characterized using a multidisciplinary approach, including physico-chemical (morphology, size distribution, FTIR) and preclinical evaluations (biocompatibility, gene expression, oxidative stress, inflammation).

2. Materials and methods

2.1. Materials

Low dextrose equivalent (DE) maltodextrin (lMD, Glucidex 2, DE = 2, MW = 9000 Da, Roquette, Giusto Faravelli, Italy) and medium dextrose equivalent maltodextrin (mMD, DE = 4.0–7.0, MW 2600–4500 Da, Sigma Aldrich, Italy) were used for microparticles preparation.

2.2. Methods

2.2.1. OMWW preparation

The olives were harvested in 2019 from the Taggiasca cultivar (Imperia, Italy) 180 days after blossom. As detailed in our previous work (Russo et al., 2022), they were processed using a semi-automatic three-phase olive processing plant located in Dolcedo (Imperia, Italy). The OMWW was previously filtered (Tagliabue et al., 2021) and subjected to vacuum membrane distillation in order to obtain a final concentrated sample. In the same work, the OMWW was analyzed for physicochemical properties, including conductivity and infrared spectroscopy, as well as total polyphenols and the antioxidant activity. The total OMWW solute content was also determined. 1 mL was dried at 70 °C up to constant weight and the solutes content was 39.9 (±0.4) %.

Three batches were prepared and samplings from each were used for microparticles production.

2.2.2. Preparation of spray-dried microparticles

Three different polymeric blends were prepared: 15 % *w/v* of lMD or mMD or 1:1 w/v lMD-mMD were added to OMWW and stirred up to complete dissolution of polysaccharides. All the samples were spray-dried using a mini spray-drier (Buchi 190, Büchi Labortechnik AG, Essen, Germany) equipped with 0.5 mm nozzle, and the process parameters were 180 °C inlet temperature, 10 % feed pump, 600 ml/h airflow and 100 % aspirator. The microparticles were collected and the process yield was always higher than 50 %.

2.2.3. Physicochemical characterization

The microparticles morphology was evaluated by means of a scanning electron microscope (SEM) Tescan, Mira3XMU (Brno, Czech Republic) after sputtering with graphite under vacuum, and were imaged at 8.0 kV. Microparticles dimensions were evaluated using a dynamic light scattering analyzer (Mastersizer 3000E, Malvern Instruments, Milan, Italy), equipped with a standard wet measurement cell. Before each measurement, the microparticles were dispersed in isopropanol and particle size parameters (d10, d50, d90, d [4,3] and Span index) were determined (Ruggeri et al., 2022b). Fourier-transform infrared (FT-IR) analysis was carried out using a Nicolet iS20 (Thermo Scientific, Italy) equipped with a DTGS detector in the range between 400 and 4000 cm^{-1} with a resolution of 4 cm^{-1}.

2.2.4. Total polyphenol content

Total polyphenol content of spray dried microparticles was determined by the Folin-Ciocalteu method (Russo et al., 2022). For this, 10 mg of powder were dissolved in 10 mL of water, and vigorously shaken. An aliquot (20 µL) was mixed with 100 µL of Folin-Ciocalteu water solution (0.2 N) and 80 µL of Na_2CO_3 solution (75 g/L). After 2 h reaction at 25 °C in the dark, the absorbance was measured at 765 nm. Total polyphenols were quantified using gallic acid calibration curve ($R^2 >$ 0.993 in the range 0.05–1 mg/mL) and were expressed as g of gallic acid equivalents (GAE) per g of sample.

2.2.5. Antioxidant activity

To evaluate the antioxidant properties, DPPH assay was performed (Ruggeri et al., 2022a). The microparticles were dissolved in water at 1 mg/mL, and 100 µL of each sample were mixed 1:1 volume ratio with DPPH methanolic solution (150 µg/mL) and incubated for 30 min in the dark. Ascorbic acid was used as positive control (200 µg/mL). The absorbance was read at 597 nm FLUOstar® Omega, (BMG LABTECH, Aylesbury, UK) and the radical scavenging activity percentages (RSA %) were calculated. Moreover, DPPH assay was also performed towards OMWW containing the same OMWW amount as the microparticles.

2.2.6. Preclinical characterization

2.2.6.1. Biocompatibility on normal human dermal fibroblasts (NHDFs). NHDFs were grown in DMEM (Dulbecco's Modified Eagle's Medium, Sigma Aldrich, Milan, Italy) supplemented with 200 IU/mL penicillin/0.2 mg/mL streptomycin (pen/strep/ampho, Euroclone, Italy) and 10 % *v*/v of a fetal bovine serum FBS (Fetal Bovine Serum, Euroclone) at 37 °C, with 5 % CO_2. Cells were plated in 96-well plates (growth area 0.36 cm^2, Greineger Bio-one, Biosigma, Italy) at a $3*10^4$ seeding density and cultured for 24 h. Then, the medium was removed and 200 µL of microparticles solutions at different concentrations (0.125–1 mg/mL) were added to each well. After 24 h of contact, the medium was removed from the wells and 100 µL of AlamarBlue (10 % v/v in DMEM) were added to each well. After 3 h of incubation at 37 °C, the fluorescence was recorded using a microplate reader (Microplate Reader Biotek, Synergy/HT, Fischer Scientific, Rodano (MI), Italy) at λ_{ex} = 530 nm and λ_{em} = 590 nm.

2.2.6.2. Evaluation of gene expression on NHDFs. NHDFs (from juvenile foreskin, PromoCell, WVR, Italy) were plated at a $1.5*10^5$ cells/well density in 48-well plates, and after 24 h 200 µL of microparticles solutions (0.5 mg/mL) were added to the wells. After 6 days of growth, NHDFs were washed, and total RNAs were isolated using TriZol agent (ThermoFisher, CA, United States) according to the manufacturer's instructions. Total RNAs were quantified by using Omega StarFluo at 230 nm. cDNA was produced using 1 µg of total RNA. Reverse transcription was carried out using iScript™ cDNA Synthesis Kit (Bio-Rad, CA, United States) according to the manufacturer's instructions. Expression of the BCL-2 and COL-1a coding RNAs was analyzed by quantitative RT-qPCR using SsoAdvanced Universal SYBR Green Supermix (Bio-Rad, CA, United States) and specific primer sets at a final concentration of 400 nM, for 50 ng of cDNA. GADPH expression was used for normalization of the RT-qPCR data. Thermal cycling program was configured as follows: polymerase activation at 95 °C for 30 s; DNA denaturation at 95 °C for 15 s and annealing at 60 °C for 30 s repeating cycles 40 times (Ruggeri et al., 2023). Finally, melt curves were recorded.

2.2.6.3. Immunofluorescence reactions. Aged NHDFs (generously provided by Bio Basic S.r.l., Pavia, Italy) were generated as previously reported (De Luca et al., 2024; Gola et al., 2023). Briefly, replicative

senescent NHDFs were induced by long-term passaging in cell culture and finally they acquired senescence phenotype at passage 48. 48 h hours before experiments, NHDFs were seeded for fluorescence analyses ($2*10^5$ cells/glass coverslip); aged fibroblasts were treated for 24 h with 100 µL of microparticles solutions at a concentration of 1 mg/mL.

Aged NHDFs cells were fixed in 4 % formalin for 20 min and post-fixed in 70 % ethanol at −20 °C for at least 24 h until staining. The cells were rehydrated for 10 min with PBS-Tween 0.2 % and then unspecific sites were blocked by using PBS solution supplemented with 2 % BSA and 0.2 % tween for 15 min at room temperature. Subsequently, samples were immunolabeled using primary antibodies (Table 1) diluted in PBS-Tween 0.2 % for 1 h, at room temperature in a moist chamber. After wash in PBS, coverslips were incubated using the respective secondary antibodies in PBS-Tween 0.2 % (1:200, Alexa Fluor, Molecular Probes, Invitrogen) for 30 min. At the end of incubation, after PBS washing, cells were counterstained for DNA with 0.1 µg/mL Hoechst 33258; then, cells were washed with PBS, and finally mounted in a drop of Mowiol (Calbiochem-Inalco S.r.l., Italy) for fluorescent microscopy. For each experimental condition, three independent experiments were carried out.

2.2.6.4. Fluorescence microscopy and image analyses. An Olympus BX51 microscope equipped with a 100-W mercury lamp was used under the following conditions: 330–385 nm excitation filter (excf), 400 nm dichroic mirror (dm) and 420 nm barrier filter (bf) for Hoechst 33258; 450–480 nm excf, 500 nm dm and 515 nm bf for the fluorescence of Alexa 488; 540 nm excf, 580 nm dm and 620 nm bf for Alexa 594.

Table 1
Primary and secondary antibodies used for fluorescence immunocytochemistry.

	Antigen	Immunogen	Dilution
Primary antibody	COX4	Mouse monoclonal [20E8C12] anti-COX4 (Abcam, Cambridge, USA)	1:200
	Catalase	Rabbit monoclonal anti-Catalase (GeneTex, Irvine, CA, USA)	1:250
	Nrf2	Rabbit polyclonal anti-Nrf2 (Abcam, Cambridge, UK)	1:200
	SOD2	Rabbit monoclonal anti-SOD2 (Cell Signaling Technology, Danvers, MA, USA)	1:200
	Anti-Mitochondria serum	Human autoimmune serum recognizing the 70 kDa E2 subunit of pyruvate dehydrogenase complex (kindly given by IRCCS San Matteo Pavia, Italy) (Ferrari et al., 2021)	1:300
	α-tubulin	Mouse monoclonal anti-Alpha-tubulin (Cell Signaling Technology, Danvers, MA, USA)	1:1000
Secondary antibody	Alexa Fluor™ 594 goat anti-human IgG (H + L) Highly Cross-Adsorbed Secondary Antibody	Gamma Immunoglobins Heavy and Light chains, Thermo Fisher Scientific (Monza, Italy)	1:200
	Alexa Fluor™ 594 goat anti-mouse IgG (H + L) Highly Cross-Adsorbed Secondary Antibody	Gamma Immunoglobins Heavy and Light chains, Thermo Fisher Scientific (Monza, Italy)	1:200
	Alexa Fluor™ 488 goat anti-mouse IgG (H + L) Highly Cross-Adsorbed Secondary Antibody	Gamma Immunoglobins Heavy and Light chains, Thermo Fisher Scientific (Monza, Italy)	1:200
	Alexa Fluor™ 488 goat anti-rabbit IgG (H + L) Highly Cross-Adsorbed Secondary Antibody	Gamma Immunoglobins Heavy and Light chains, Thermo Fisher Scientific (Monza, Italy)	1:200

Images were recorded with an Olympus MagniFire camera system and processed with the Olympus Cell F software (version n. v3.1).

After immunocytochemistry, images were acquired using Cell F software. Time exposure during acquisition was determined on control cells and then maintained for all the experimental conditions, to compare fluorescence intensity between different experimental groups. The cell fluorescence intensity was measured using ImageJ software 1.51 (NIH, MA, USA).

2.2.6.5. Biocompatibility on macrophages and nitric oxide assay. Cytocompatibility assay was carried out using macrophages (Raw 264.7 murine macrophages, Sigma-Aldrich, Italy). The cells were grown at 37 °C in a DMEM medium and cultured with a seeding density of $25*10^3$ cells/well in a 96-well. After 24 h of growth, 200 µL of microparticles at different concentrations (0.125–1 mg/mL) were added to each well. After 24 h of contact, AlamarBlue assay was performed as previously described.

The nitric oxide assay was also performed. After incubation of macrophages ($25*10^3$ cells/well) with 1 µg/mL lipopolysaccharide (LPS) for 3 h, cells were treated with 100 µL of microparticles solutions at a concentration of 1 mg/mL in DMEM w/o phenol red for 6 h. Afterwards, 100 µL of cell culture media were mixed with 100 µL of Griess reagent (1 % *v*/v sulfanilamide and 0.1 % v/v naphthylethylenediamine dihydrochloride in 2.5 % phosphoric acid). Finally, after 15 min of contact, the absorbance was measured at 540 nm, and NO amount was determined from a standard curve of sodium nitrite ($NaNO_2$) ($R^2 > 0.995$ in the range 65–0.45 µM) (Yang et al., 2009).

2.2.6.6. Statistical analysis. Statistical analysis was performed using Astatsa statistical calculator. 1-way Anova was followed by Scheffè for post-hoc comnparison. As previously described (Ratto et al., 2020), immunochemical results were expressed as mean ± sd. Briefly, for data passed the normality test D'Agostino & Pearson test, Anderson-Darling test, Shapiro-Wilk test and Kolmogorov-Smirnov test the analysis was conducted using Unpaired *t*-test. Diversely, for non-normally distributed results, the analysis was performed employing Mann-Whitney test GraphPad Prism 9.0 (GraphPad Software Inc., CA, USA) $p < 0.05$ was considered statistically significant.

3. Results and discussions

3.1. Physico-chemical characterization

Many studies highlight the health benefits of extra virgin olive oil (EVO). However, during extraction, the physicochemical properties of water-soluble phenolics cause differential partitioning between oil and water. In fact, the majority (about 98 %) of these phenolic compounds, known for their remarkable radical scavenging activities, are transferred from the olive pulp to the waste byproducts. Consequently, OMWW represents an interesting waste product. In this study, OMWW was encapsulated into microparticles using maltodextrins, through spray-drying.

Fig. 1a shows the SEM micrographs of OMWW-based spray-dried microparticles, and Fig. 1b displays the particle size parameters. The morphological analysis reveals a smooth, spherical shape with no surface defects. Additionally, the morphology appears unaffected by the dextrose equivalents (DE) of the maltodextrins. Similar morphological characteristics were reported in previous studies by Paulo and coworkers (Paulo et al., 2022). The microparticles have a mean diameter in the range of 17–18.9 µm and a narrow size distribution, as indicated by the span factor ranging from 1.55 to 1.63. The slight differences in microparticle size could be related to the different DE values, and consequently, the molecular weight of the maltodextrins used. Specifically, a higher DE corresponds to a lower molecular weight. Microparticles based on low DE maltodextrins (lMD) have a greater diameter

A)

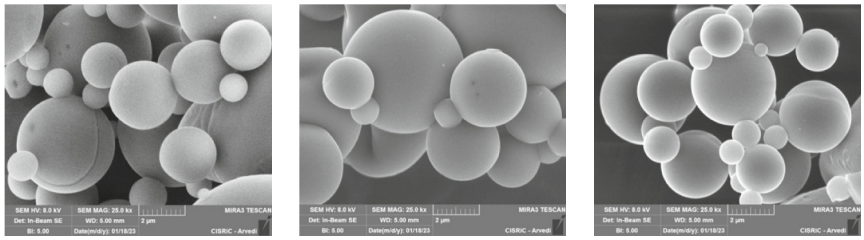

B)

	d10 (μm)	d50 (μm)	d90 (μm)	d[4;3] (μm)	Span Index
IMD	6.8±0.4	16.7±0.2	34±0.8	18.7±0.2	1.6±0.1
mMD	6.3±0.2	15.4± 0.5	30.3±2.5	17±0.9	1.6±0.1
lMD-mMD	6.7±0.2	15.9±0.4	31.9±2.7	17.8±0.9	1.6±0.2

Fig. 1. a) SEM micrographs of spray-dried microparticles; b) particle size (d10, d50, d90, d[4;3], Span Index) (mean ± s.d.; $n = 6$). ANOVA one-way; Sheffe' test ($p < 0.05$) d[4; 3]: lMD vs. mMD; lMD vs. lMD-mMD; mMD vs. lMD-mMD.

than those based on medium DE (mMD) and low-medium DE (lMD-mMD) maltodextrins. This difference is likely due to the chemical-physical properties of the polymeric mixture used. Higher molecular weight polymers result in higher viscosity blends, leading to the formation of larger droplets during atomization and, consequently, larger microparticles.

Fig. 2 shows the FTIR spectra of pristine components (left panel) and spray-dried microparticles (right panel). The spectrum of pristine OMWW exhibits a broad band between 3600 and 3000 cm^{-1}, corresponding to the stretching vibrations of hydroxyl groups. Additionally, absorption peaks around 2925 cm^{-1} are attributed to the stretching vibrations of CH bonds, indicating the presence of alkanes and alkyl chains in lipids. The shoulder peak at 1752 cm^{-1} corresponds to the vibrations of carbonyl groups (C=O), carboxyl, ketone groups, and esters. Bands in the range of 1600–1400 cm^{-1} indicate the presence of carboxylate groups (-COO-) from fatty acids and organic acids, as well as the bending vibrations of aromatic C—H bonds found in phenolic compounds, such as polyphenols. Moreover, the broad peak at 1061 cm^{-1} is related to vibrations in carbohydrates (Raji et al., 2023).

Pristine low and medium DE maltodextrins display similar FTIR spectra, characterized by a wide region between 3200 and 3550 cm^{-1} related to hydroxyl group stretching. In the case of spray-dried microparticles, the spectra of all samples exhibit features of both pristine OMWW and maltodextrin. This suggests that there are no strong chemical interactions between OMWW and maltodextrins, as no significant changes in the FTIR spectra are observed. Consequently, it can be inferred that the encapsulation process does not impair the stability of OMWW.

3.2. Total polyphenol content and antioxidant activity

Fig. 3A shows the total polyphenol content, expressed as g of gallic acid equivalents per g of sample, providing insights into the concentration of these bioactive molecules in OMWW and OMWW-loaded microparticles. Regardless of the type of maltodextrin used, the polyphenol content in the microparticles remains consistent with that of the original OMWW. This indicates that the spray drying process and the use of maltodextrins as polymeric matrices effectively preserve the phenolic concentration and stability of OMWW.

The antioxidant properties were assessed via the DPPH assay, as shown in Fig. 3B. The radical scavenging activities (RSA %) of the microparticles were measured, using ascorbic acid as a positive control (C+) due to its well-known antioxidant properties. All developed microparticles demonstrated significant antioxidant activity by inhibiting free radicals. This notable antioxidant activity is primarily attributed to the polyphenolic compounds in OMWW, as previously described in the literature, which reported a performance comparable to or even higher than other natural antioxidants like vitamin C or Trolox (Dahmen-Ben Moussa et al., 2021). All the OMWW batches used show comparable activities, suggesting the process reproducibility of the OMWW. The antioxidant activity of OMWW is mainly attributed to hydroxytyrosol (10–25 %), flavonoids (6–19 %) and secoiridoid derivatives (13–27 %) (Leouifoudi et al., 2014), while the other components of OMWW are unsaturated fatty acids, polysaccharides, and proteins. This makes these

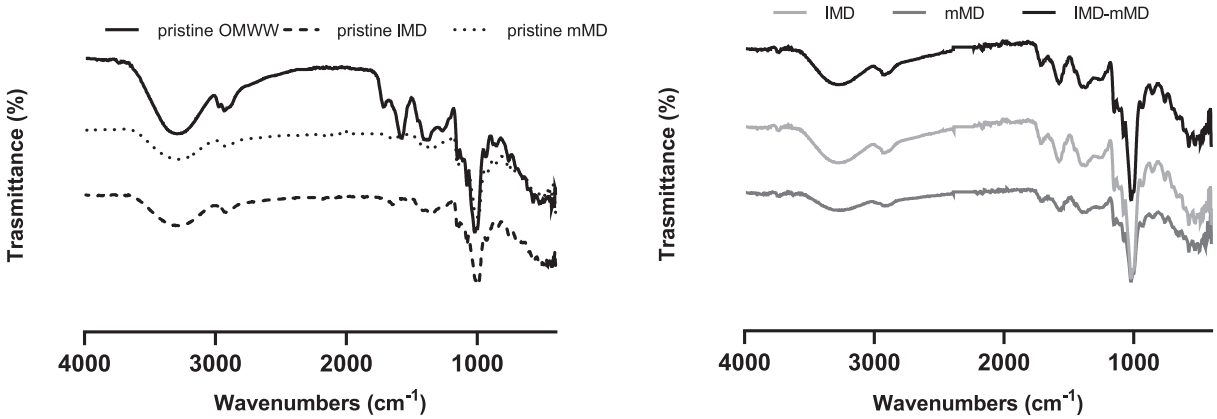

Fig. 2. FTIR spectra of pristine components (left panel) and spray-dried microparticles (right panel).

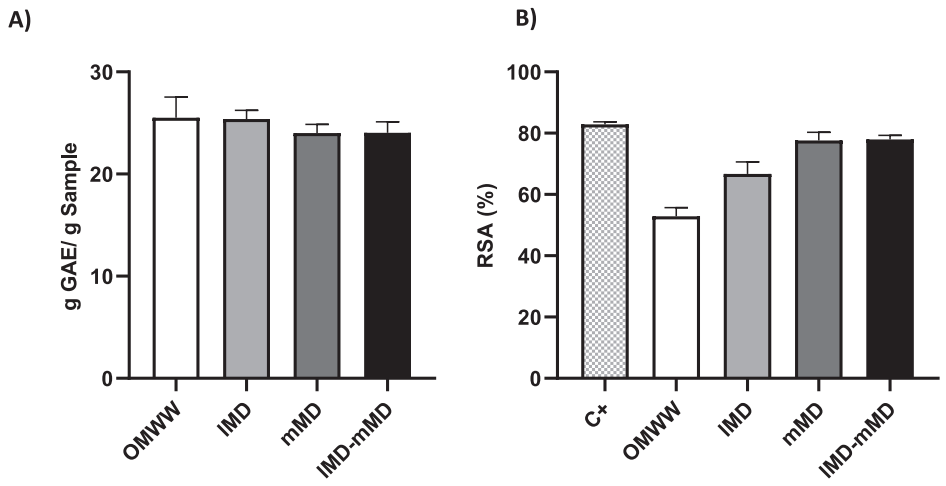

Fig. 3. A) Total polyphenol content (g GAE/ g of sample) of the microparticles (mean values ± s.d.; $n = 3$); B) radical scavenging activity (RSA %) of ascorbic acid (C+, positive control), OMWW, and microparticles (mean values ± s.d.; $n = 3$). ANOVA one-way; Sheffe' test ($p < 0.05$): C+ vs OMWW; C+ vs. lMD; OMWW vs. lMD; OMWW vs. mMD; OMWW vs. lMD-mMD; lMD vs. mMD; lMD vs. lMD-mMD.

microparticles promising candidates for various applications, as they could play a crucial role in neutralizing free radicals and oxidative stress, thereby protecting cells from damage and reducing the risk of chronic diseases. Moreover, the results suggest that maltodextrin (MD) contributes to the antioxidant properties of the microparticles, which are significantly higher than those of pristine OMWW. The properties of MD depend on its molecular weight, with lower molecular weight maltodextrins (mMD) showing the best performance. The results also indicated that microparticles with medium DE maltodextrins (mMD) and low-medium DE maltodextrins (lMD-mMD) exhibited radical scavenging activities comparable to the positive control. This could be related to the DE of maltodextrin, which affects the stability of encapsulated bioactive molecules. Lower DE values result in longer polymer chains, leading to slower degradation, while higher DE values yield shorter chains with faster degradation, making the polyphenolic compounds more accessible. Interestingly, the microparticles showed significantly higher antioxidant activity than pristine OMWW ($p < 0.05$). This could be related to the process occurring at high temperature (180 °C). Although the heating is extremely short and basically allow the water evaporation at 100 °C, it could trigger the Maillard reaction, and the formation of the related products characterized by antioxidant properties (Ruggeri et al., 2022a). Similar findings were reported by Bushra Sultana et al. (Bushra Sultana, 2012), who observed increased antioxidant activity in oven-dried apricot fruit compared to fresh fruit, likely due to the formation of Maillard reaction products and the release of bound phenolics into simpler free forms. However, the relationship between polyphenol content and antioxidant activity during dehydration remains complex, influenced by variables such as drying technique, antioxidant tests, and interactions among various antioxidant reactions (Miranda et al., 2010).

The antioxidant activity of OMWW is mainly attributed to hydroxytyrosol (10–25 %), flavonoids (6–19 %) and secoiridoid derivatives (13–27 %) (Leouifoudi et al., 2014), while the other components of OMWW are unsaturated fatty acids, polysaccharides, and proteins.

3.3. Cell biocompatibility and gene expression

Fig. 4A shows the cell viability percentages of fibroblasts after incubation with microparticles. All microparticles were compared to a positive control where cells were seeded at the bottom of the wells and grown under standard conditions. Overall, the microparticles demonstrated biocompatibility at concentrations below 1 mg/mL, exhibiting similar behavior to the positive control. However, at higher concentrations, a decrease in cell viability was observed. This decrease could be attributed to the high concentration of OMWW salts, which may affect cell metabolism and inhibit cell growth.

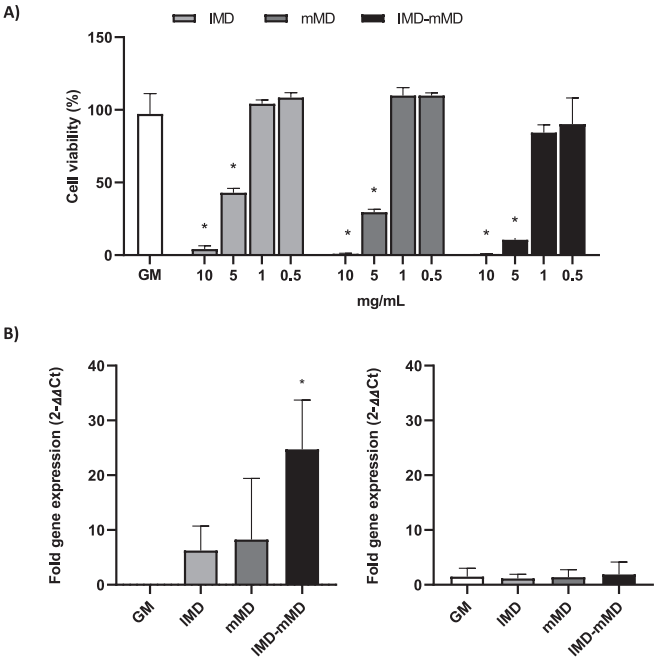

Fig. 4. A) Cell viability percentages of NHDFs after 24 h of contact with microparticles in comparison to the positive control GM (growth medium, as standard growth conditions) (mean values ± s.d.; $n = 5$). Values * are statistically significant ($p < 0.05$) compared with GM. B) Bcl-2 (left panel) and Col-1a (right panel) expression of fibroblasts after 7 days of contact with the mycelia extracts (mean values ± sd; n = 3). Values * are statistically significant ($p < 0.05$) compared with GM.

Additionally, the ability of the microparticles to promote gene expression in normal human dermal fibroblasts (NHDFs) was investigated using rt-qPCR. Specifically, the expression of extracellular matrix protein (collagen) and proliferation/apoptotic stimulus (Bcl-2) was evaluated. Fig. 4B presents Col-1α (left panel) and Bcl-2 (right panel) gene fold expression in NHDFs grown for 6 days in contact with the microparticles, with cells grown under standard conditions, as the control. Col-1α is associated with extracellular matrix production and deposition, while Bcl-2 is an anti-apoptotic gene that describes the cells'

apoptotic activity.

The expression of Col-1α in cells grown in contact with the microparticles showed a statistically significant increase compared to the control sample. Both low DE (lMD) and medium DE (mMD) maltodextrins modulated collagen production to levels higher than the control, while the combination of both maltodextrins further enhanced Col-1α expression, showing an increase of about 18-fold compared to the control. Conversely, the mRNA expression levels of Bcl-2 did not show statistically significant differences from the control samples, suggesting that the microparticles do not induce mitotic/apoptotic activity.

Previous studies have reported that polyphenols can regulate gene expression. Hydroxytyrosol has been shown to modulate Bcl-2 expression by forming a stable bond with its hydrophobic groove (Verma et al., 2017; Zubair et al., 2017), while oleuropein, a polyphenol commonly found in OMWW, appears to be involved in the up-regulation of Col-1α (Tagliaferri et al., 2014).

3.4. Immunofluorescence reactions

Aged human neonatal dermal fibroblasts (NHDFs) were also used to evaluate the effect of OMWW-encapsulated microparticles on the oxidative stress pathway in senescent fibroblasts, an in vitro model characterized by physiological reactive oxygen species (ROS) overproduction (Gola et al., 2023)). To assess the possible modulatory effects of the microparticles on the oxidative stress pathway, immunofluorescence reactions were performed on control and differently treated old-NHDF cells. Specifically, alterations in the expression levels of oxidative stress markers (COX4, catalase, Nrf2, and SOD2) and cellular organelles (mitochondria and α-tubulin) were evaluated.

Fig. 5 shows the double immunofluorescence reaction for mitochondria (red signal) and COX4 (green signal) in the reference (GM) (a-c) and microparticle-treated NHDF cells (d-f, g-i, and j-l for lMD, mMD, and lMD-mMD, respectively). In all experimental groups, both mitochondria and COX4 fluorescence signals are homogeneously distributed

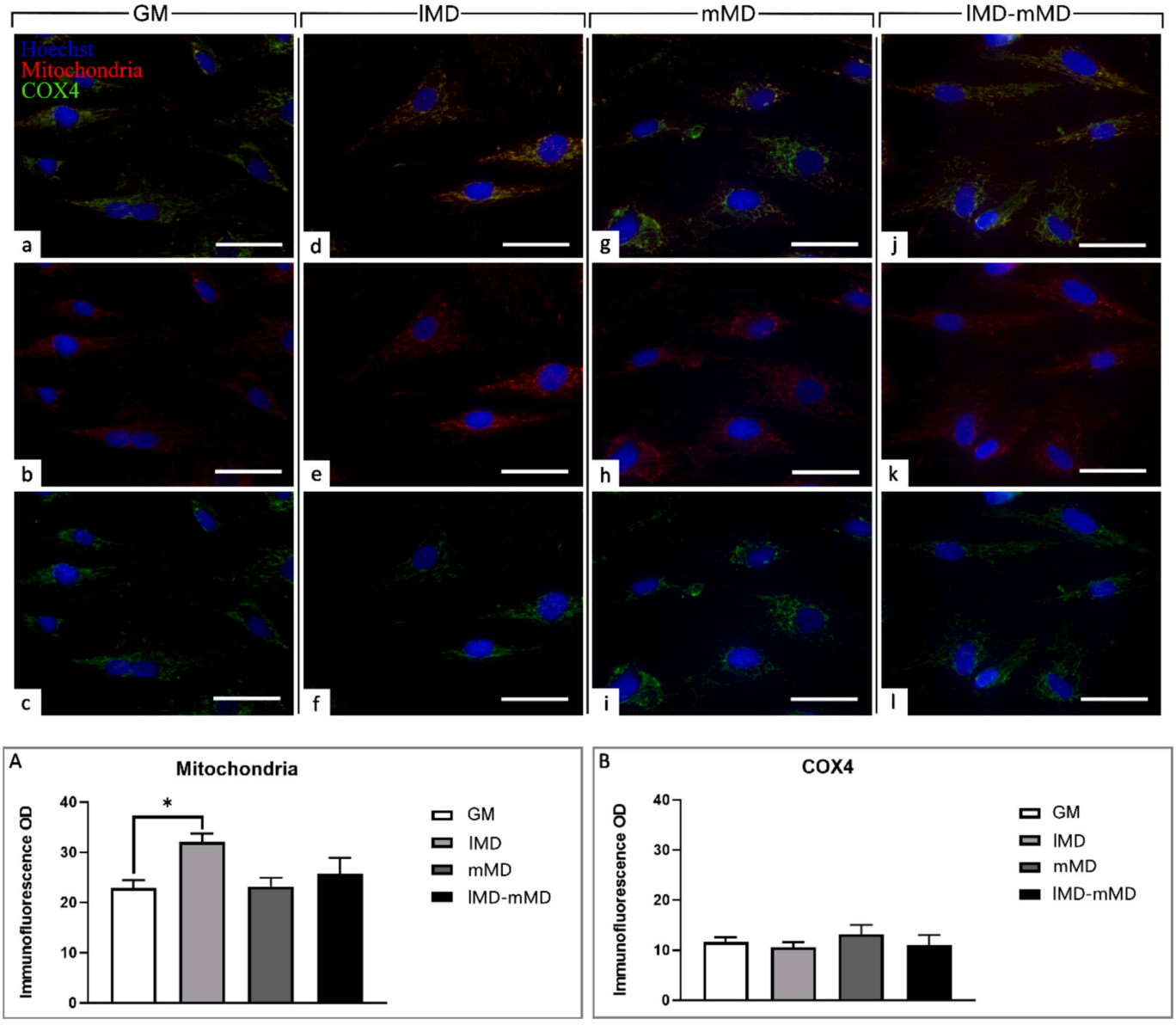

Fig. 5. Double immunofluorescence reaction for mitochondria (red signal) and COX4 (green signal) in GM (a-c), lMD (d-f), mMD (g-i) and lMD-mMD (j-l) treated old NHDF cells. DNA counterstaining with Hoechst 33258 (blue fluorescence). Histograms showing the quantitative analyses of mitochondria (Panel A) and COX4 (Panel B) mean fluorescence intensity per cell. Statistically significant data: $*p < 0.05$. Magnification: 40×. Scale bars: 50 μm. (For interpretation of the references to colour in this figure legend, the reader is referred to the web version of this article.)

in the cell cytoplasm, with partial colocalization in lMD and lMD-mMD treated cells (orange signal).

Immunoreaction for mitochondria reveals a statistically significant increase in immunopositive optical density (OD) in lMD-treated cells compared to the contraol (GM). No significant difference is observed when comparing lMD with mMD or lMD-mMD. A slight increase in mitochondrial signal is observed in both mMD and lMD-mMD treated cells compared to the control group (GM) (Fig. 5, Panel A). However, quantitative analysis of COX4 immunopositive OD shows a similar trend of enzyme expression levels across all experimental groups, without any significant differences in COX4 immunopositive OD (Fig. 5, Panel B).

Fig. 6 shows the double immunofluorescence for α-tubulin (red signal) and catalase (green signal) in the control (GM) (a-c) and microparticle-treated NHDF cells (d-f, g-i, and j-l for lMD, mMD, and lMD-mMD, respectively). The cytoskeleton maintains its physiological organization in all experimental groups, characterized by homogeneous and well-distributed immunopositivity for α-tubulin throughout the entire cytoplasmic compartment, clearly visible as filamentous, aggregate-free immunofluorescence. Parallelly, catalase immunolabeling is detectable as green fluorescence spots distributed in the cytoplasm, usually localized at the perinuclear level.

Immunofluorescence analysis of α-tubulin reveals no significant differences in fluorescence optical density (OD) between all experimental groups (Fig. 6A). However, immunoreaction for catalase highlights a statistically significant decrease in immunopositive OD in cells treated with both lMD and lMD-mMD microparticles compared to the control (GM). No significant difference is observed when comparing mMD-treated cells to the control (GM) or between lMD and lMD-mMD-treated NHDF cells (Fig. 6B).

Fig. 7 shows the double immunofluorescence reaction for α-tubulin (red signal) and Nrf2 (green signal) in the control group (GM) (a-c) and microparticle-treated NHDF cells (d-f, g-i, and j-l for lMD, mMD, and lMD-mMD, respectively). Similar to the observations from the catalase immunofluorescence reaction, the cytoskeleton exhibits well-preserved organization across all samples, characterized by filamentous cytoplasmic α-tubulin immunopositivity. Nrf2 immunopositivity, in contrast, is strongly confined to the nucleus and clearly detectable as immunofluorescence spots.

Analysis of α-tubulin immunofluorescence OD reveals no significant differences between all experimental groups (Fig. 7A). In parallel, Nrf2 immunofluorescence shows a significant decrease in immunopositive OD in cells treated with lMD microparticles compared to the control

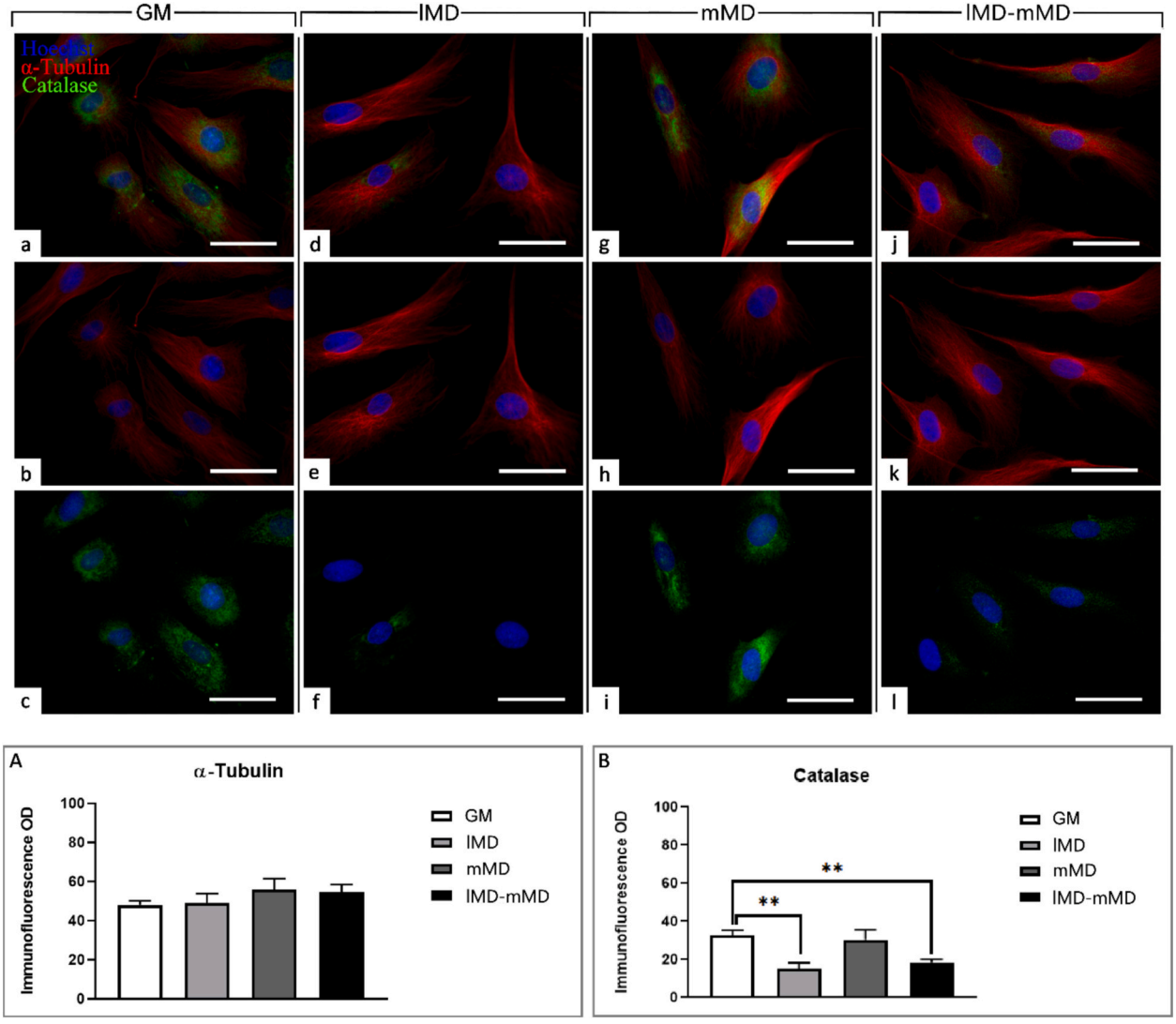

Fig. 6. Double immunofluorescence reaction for α-tubulin (red signal) and catalase (green signal) in GM (a-c), lMD (d-f), mMD (g-i) and lMD-mMD (j-l) treated old NHDF cells. DNA counterstaining with Hoechst 33258 (blue fluorescence). Histograms showing the quantitative analyses of α-tubulin (Panel A) and catalase (Panel B) mean fluorescence intensity per cell. Statistically significant data: $^{**}p < 0.01$. Magnification: 40×. Scale bars: 50 μm. (For interpretation of the references to colour in this figure legend, the reader is referred to the web version of this article.)

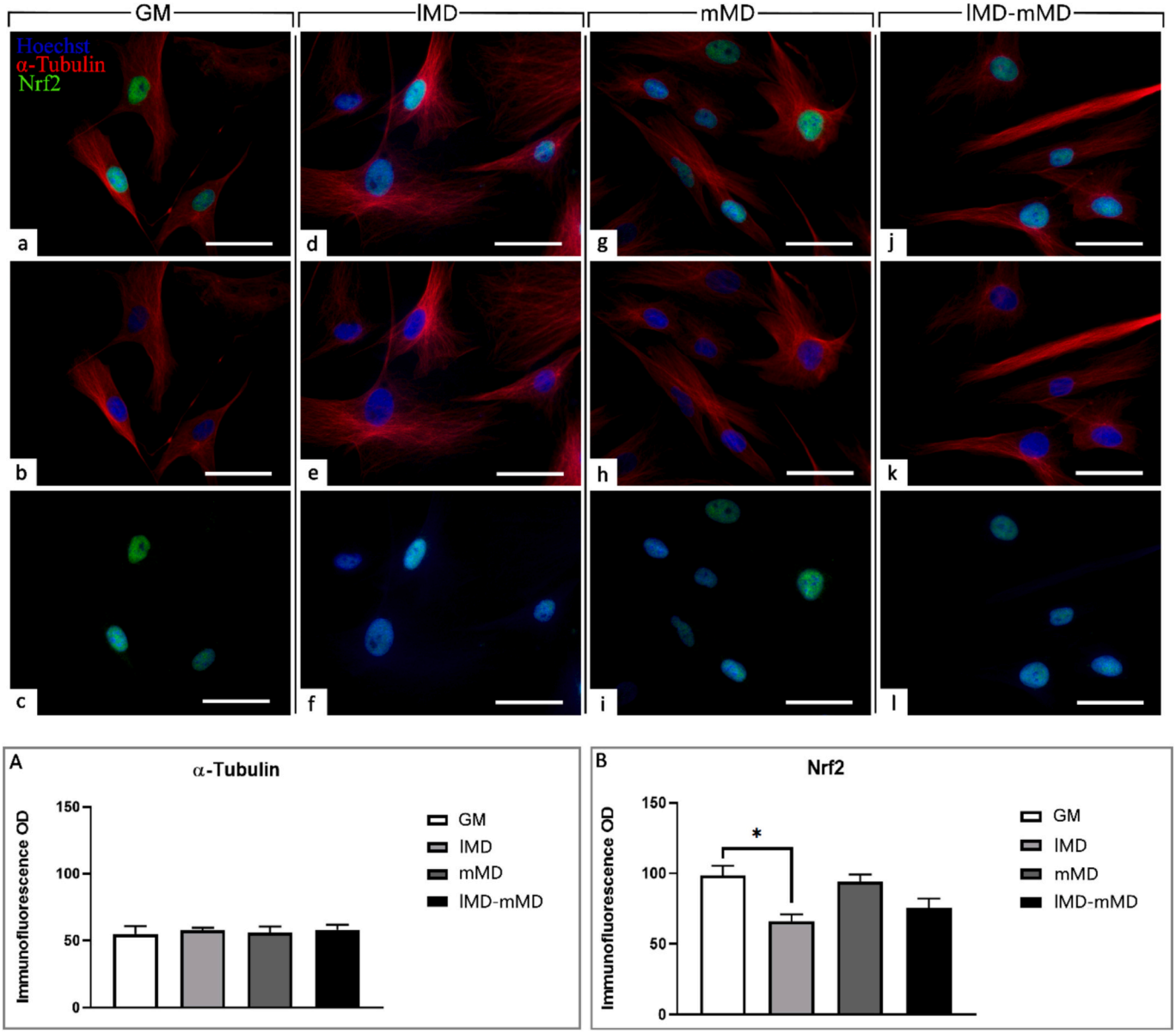

Fig. 7. Double immunofluorescence reaction for α-tubulin (red signal) and Nrf2 (green signal) in GM (a-c), lMD (d-f), mMD (g-i) and lMD-mMD (j-l) treated old NHDF cells. DNA counterstaining with Hoechst 33258 (blue fluorescence). Histograms showing the quantitative analyses of α-tubulin (Panel A) and Nrf2 (Panel B) mean fluorescence intensity per cell. Statistically significant data: $^{*}p < 0.05$. Magnification: 40×. Scale bars: 50 μm. (For interpretation of the references to colour in this figure legend, the reader is referred to the web version of this article.)

(GM). However, only a slight, non-statistically significant decrease is observed when comparing mMD and lMD-mMD treated cells to the control (GM), or between lMD-mMD and mMD treated cells (Fig. 7B).

Fig. 8 reports the double immunofluorescence results for mitochondria (red signal) and SOD2 (green signal) in the control group (GM) (a-c) and microparticle-treated NHDF cells (d-f, g-i, and j-l for lMD, mMD, and lMD-mMD, respectively). In all experimental groups, mitochondria and SOD2 are homogeneously distributed in the cell cytoplasm and are clearly detectable as immunopositive fluorescent spots. A slight colocalization of mitochondria and SOD2 immunopositivity (orange signal) is observed, with varying degrees in the treated NHDF cells. Similar to the previous immunofluorescence results for COX4, a statistically significant increase in mitochondrial immunopositive OD is detected only in lMD-treated cells compared to the control (GM) (Fig. 8A). Additionally, the quantitative analysis of SOD2 immunofluorescence OD reveals no significant differences between experimental groups. The observed slight changes in SOD2 OD are likely due to physiological variability (Fig. 8B).

3.5. Biocompatibility on macrophages and nitric oxide assay

Fig. 9A reports the cell viability percentages of macrophages. Consistent with previous observations in fibroblasts, the microparticles demonstrate safety at concentrations below 1 mg/mL, with cell viability comparable to the positive control. However, at higher concentrations, there is a decrease in cell viability, similar to what was observed in fibroblasts. Furthermore, the effects of the microparticles on proinflammatory mediators secreted from murine macrophages were investigated. Fig. 9B displays the percentage of NO production in LPS-stimulated macrophages after exposure to spray-dried microparticles. The results indicate that all samples exhibit significantly lower NO production compared to LPS, used as positive control. This finding is noteworthy because nitric oxide (NO) is a crucial signaling molecule involved in various physiological processes such as neurotransmission, vasodilation, and neurotoxicity (Ahmed et al., 2022). However, excessive NO production is associated with autoimmune and inflammatory

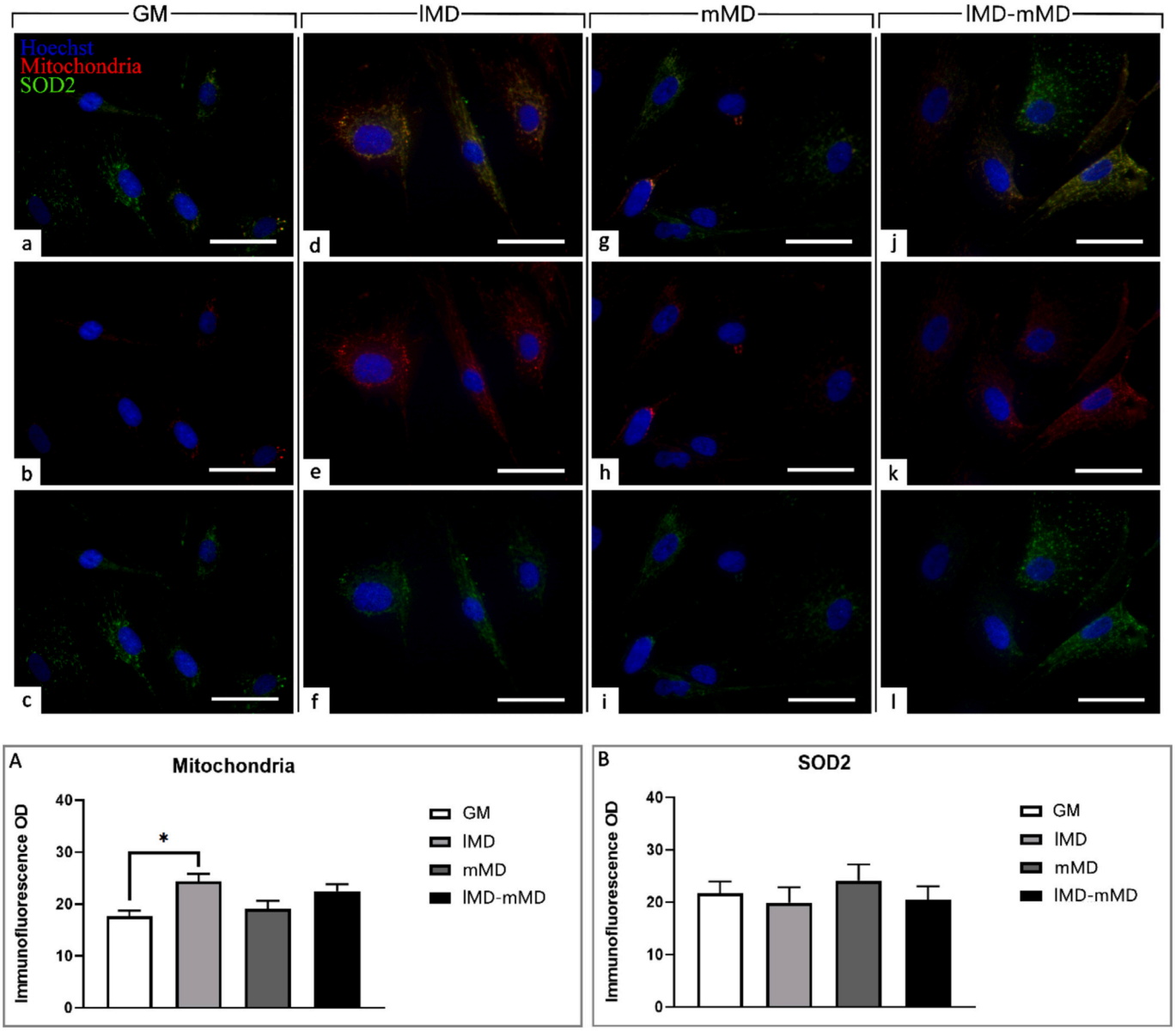

Fig. 8. Double immunofluorescence reaction for mitochondria (red signal) and SOD2 (green signal) in GM (a-c), lMD (d-f), mMD (g-i) and lMD-mMD (j-l) treated old NHDF cells. DNA counterstaining with Hoechst 33258 (blue fluorescence). Histograms showing the quantitative analyses of mitochondria (Panel A) and SOD2 (Panel B) mean fluorescence intensity per cell. Statistically significant data: $*p < 0.05$. Magnification: 40×. Scale bars: 50 μm. (For interpretation of the references to colour in this figure legend, the reader is referred to the web version of this article.)

diseases, highlighting the anti-inflammatory effects of these microparticles by reducing NO generation.

4. Conclusions

The study detailed in this work explores the encapsulation of olive mill wastewater into microparticles using maltodextrins via spray-drying, focusing on their physicochemical properties, antioxidant potential, and biological effects. One innovative aspect lies in the effective encapsulation of OMWW, which is rich in bioactive polyphenols, into stable microparticles without compromising their antioxidant capacity. The microparticles exhibited a smooth morphology and uniform size distribution.

Moreover, the study highlights the antioxidant efficacy of these microparticles, showing significant radical scavenging activity comparable to or exceeding that of traditional antioxidants. This underscores their potential in mitigating oxidative stress-related damage, thereby potentially reducing the risk of chronic diseases associated with oxidative stress.

Furthermore, the biocompatibility assessment using fibroblasts and macrophages revealed that the microparticles are safe at lower concentrations and exhibited cell viability similar to control conditions. This aspect is crucial for their potential applications in biomedical and pharmaceutical fields where biocompatibility is a prerequisite.

In conclusion, the encapsulation of OMWW into maltodextrin-based microparticles through spray-drying represents a promising approach to harnessing the bioactive potential of OMWW. These microparticles not only preserve the polyphenolic compounds but also enhance their stability and bioavailability. The significant antioxidant activity demonstrated by the microparticles suggests their potential application as natural antioxidants in wound healing. Moreover, the observed anti-inflammatory effects, indicated by reduced nitric oxide (NO) production in macrophages, further enhance the attractiveness of these microparticles for applications in facing inflammatory conditions. Overall,

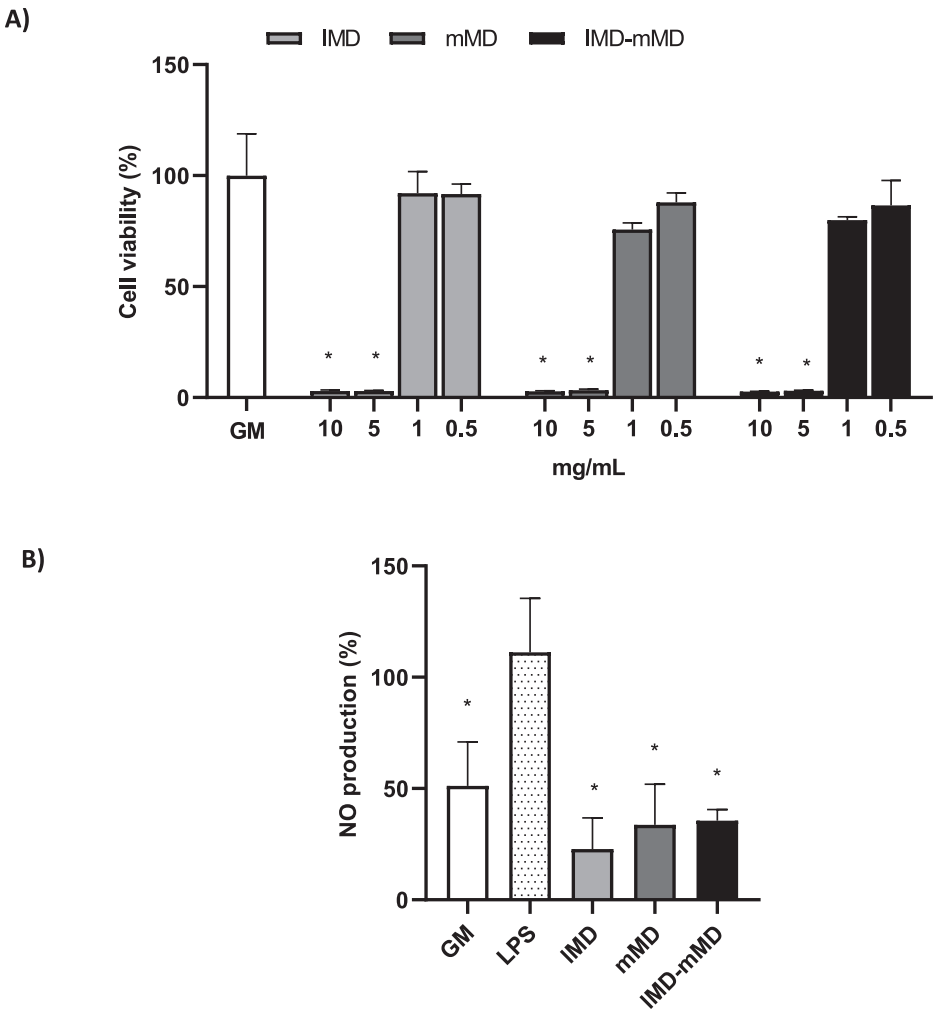

Fig. 9. A) Cytocompatibility of macrophages (cell viability percentages) after 24 h of contact with spray dried microparticles (mean values ± sd; $n = 5$). Values * are statistically significant ($p < 0.05$) compared with control. B) Nitrite (NO) production in LPS-stimulated macrophages (mean values ± sd; $n = 3$). Values * indicate significant differences ($p < 0.05$) respect to LPS.

this study contributes to offer sustainable high-value products for valorizing agricultural by-products like OMWW while addressing pressing health and environmental challenges.

CRediT authorship contribution statement

Marco Ruggeri: Writing – review & editing, Writing – original draft, Methodology, Formal analysis, Investigation, Data curation, Conceptualization, Supervision. **Fabrizio De Luca:** Investigation, Data curation. **Amedeo Ungolo:** Visualization, Formal analysis, Investigation, Data curation. **Barbara Vigani:** Visualization, Formal analysis. **Alejandro J. Paredes:** Validation. **Eleonora Russo:** Resources. **Maria Grazia Bottone:** Resources. **Eleonora Bianchi:** visualization; **Franca Ferrari:** validation, resources; **Silvia Rossi:** Validation, Resources. **Giuseppina Sandri:** Writing – review & editing, Conceptualization, Project administration, Resources, Funding acquisition.

Declaration of competing interest

The authors declare the following financial interests/personal relationships which may be considered as potential competing interests:

Giuseppina Sandri reports financial support was provided by The National Recovery and Resilience Plan (NRRP). If there are other authors, they declare that they have no known competing financial interests or personal relationships that could have appeared to influence the work reported in this paper.

Data availability

Data will be made available on request.

Acknowledgments

This research was funded by the National Recovery and Resilience Plan (NRRP), Mission 4 Component 2 Investment 1.3—Call for proposals No. 341 of 15 March 2022 of Italian Ministry of University and Research funded by the European Union—NextGenerationEU, Award Number: Project code PE00000003, Concession Decree No. 1550 of 11 October 2022 adopted by the Italian Ministry of University and Research, CUP D93C22000890001, Project title “ON Foods—Research and innovation network on food and nutrition Sustainability, Safety and Security—Working ON Foods”. This project was also supported by NRRP M4 – Ecosistemi d’innovazione NODES – Nord Ovest Digitale E Sostenibile. Alejandro Paredes was a CICOPS Fellow.

References

Aggoun, M., Arhab, R., Cornu, A., Portelli, J., Barkat, M., Graulet, B., 2016. Olive mill wastewater microconstituents composition according to olive variety and extraction process. Food Chem. 209, 72–80. https://doi.org/10.1016/j.foodchem.2016.04.034.

Ahmed, R., Augustine, R., Chaudhry, M., Akhtar, U.A., Zahid, A.A., Tariq, M., Falahati, M., Ahmad, I.S., Hasan, A., 2022. Nitric oxide-releasing biomaterials for promoting wound healing in impaired diabetic wounds: state of the art and recent trends. Biomed. Pharmacother. 149, 112707. https://doi.org/10.1016/j.biopha.2022.112707.

Alkhalidi, A., Halaweh, G., Khawaja, M.K., 2023. Recommendations for olive mills waste treatment in hot and dry climate. J. Saudi Soc. Agric. Sci. 22, 361–373. https://doi.org/10.1016/j.jssas.2023.03.002.

Al-Qodah, Z., Al-Zoubi, H., Hudaib, B., Omar, W., Soleimani, M., Abu-Romman, S., Frontistis, Z., 2022. Sustainable vs. conventional approach for olive oil wastewater management: a review of the state of the art. Water (Switzerland). https://doi.org/10.3390/w14111695.

Bilal, R.M., Liu, C., Zhao, H., Wang, Y., Farag, M.R., Alagawany, M., Hassan, F.U., Elnesr, S.S., Elwan, H.A.M., Qiu, H., Lin, Q., 2021. Olive oil: nutritional applications, beneficial health aspects and its prospective application in poultry production. Front. Pharmacol. https://doi.org/10.3389/fphar.2021.723040.

Bushra Sultana, 2012. Effect of drying techniques on the total phenolic contents and antioxidant activity of selected fruits. J. Med. Plant Res. 6. https://doi.org/10.5897/jmpr11.916.

Carmona, I., Aguirre, I., Griffith, D.M., García-Borrego, A., 2023. Towards a circular economy in virgin olive oil production: valorization of the olive mill waste (OMW) “alpeorujo” through polyphenol recovery with natural deep eutectic solvents (NADESs) and vermicomposting. Sci. Total Environ. 10 (872), 162198. https://doi.org/10.1016/j.scitotenv.2023.162198.

Christoforou, E., Fokaides, P.A., 2016. A review of olive mill solid wastes to energy utilization techniques. Waste Manag. 49, 346–363. https://doi.org/10.1016/j.wasman.2016.01.012.

Dahmen-Ben Moussa, I., Maalej, A., Masmoudi, M.A., Feki, F., Choura, S., Baccar, N., Jelail, L., Karray, F., Chamkha, M., Sayadi, S., 2021. Effect of olive mill wastewaters on Scenedesmus sp. growth, metabolism and polyphenols removal. J. Sci. Food Agric. 101, 5508–5519. https://doi.org/10.1002/jsfa.11200.

De Luca, F., Gola, F., Azzalin, A., Casali, C., Gaiaschi, L., Milanesi, G., Vicini, R., Rossi, P., Bottone, M.G., 2024. A Lombard variety of sweet pepper regulating senescence and proliferation: the Voghera pepper. Nutrients 16, 1681. https://doi.org/10.3390/nu16111681.

Ferrari, B., Roda, E., Priori, E.C., De Luca, F., Facoetti, A., Ravera, M., Brandalise, F., Locatelli, C.A., Rossi, P., Bottone, M.G., 2021. A new platinum-based prodrug candidate for chemotherapy and its synergistic effect with hadrontherapy: novel strategy to treat glioblastoma. Front. Neurosci. 15. https://doi.org/10.3389/fnins.2021.589906.

Gola, F., Gaiaschi, L., Roda, E., De Luca, F., Ferulli, F., Vicini, R., Rossi, P., Bottone, M.G., 2023. Voghera sweet pepper: a potential ally against oxidative stress and aging. Int. J. Mol. Sci. 24. https://doi.org/10.3390/ijms24043782.

Leouifoudi, I., Zyad, A., Amechrou, Q.A., Oukerrou, M.A., Mouse, H.A., Mbarki, M., 2014. Identification and characterisation of phenolic compounds extracted from Moroccan olive mill wastewater. Food Sci. Technol. Camp. 34, 249–257. https://doi.org/10.1590/fst.2014.0051.

Mechnou, I., Meskini, S., Raji, Y., Kouar, J., Hlaibi, M., 2023. Development of a novel in-situ aluminum/carbon composite from olive mill wastewater for the selective adsorption and separation of malachite green and acid yellow 61. Bioresour. Technol. 384, 129272. https://doi.org/10.1016/j.biortech.2023.129272.

Mechnou, I., Meskini, S., Elqars, E., Ait El Had, M., Hlaibi, M., 2024. Efficient CO2 capture using a novel Zn-doped activated carbon developed from agricultural liquid biomass: adsorption study, mechanism and transition state. Surf. Interf. 52, 104846. https://doi.org/10.1016/j.surfin.2024.104846.

Miranda, M., Vega-Gálvez, A., López, J., Parada, G., Sanders, M., Aranda, M., Uribe, E., Di Scala, K., 2010. Impact of air-drying temperature on nutritional properties, total phenolic content and antioxidant capacity of quinoa seeds (*Chenopodium quinoa* Willd.). Ind. Crop. Prod. 32, 258–263. https://doi.org/10.1016/j.indcrop.2010.04.019.

Moglie, M., Biancini, G., Norici, A., Mugnini, A., Cioccolanti, L., 2024. Valorization of olive mill wastewater for Arthrospira platensis production. Cell Rep. Sustain. 1, 100017. https://doi.org/10.1016/j.crsus.2024.100017.

Nunes, A.M., Costa, A.S.G., Bessada, S., Santos, J., Puga, H., Alves, R.C., Freitas, V., Oliveira, M.B.P.P., 2018. Olive pomace as a valuable source of bioactive compounds: a study regarding its lipid- and water-soluble components. Sci. Total Environ. 644, 229–236. https://doi.org/10.1016/j.scitotenv.2018.06.350.

Paulo, F., Tavares, L., Santos, L., 2022. Extraction and encapsulation of bioactive compounds from olive mill pomace: influence of loading content on the physicochemical and structural properties of microparticles. J. Food Meas. Charact. 16, 3077–3094. https://doi.org/10.1007/s11694-022-01408-z.

Raji, Y., Nadi, A., Chemchame, Y., et al., 2023. Eco-friendly extraction of flavonoids dyes from Moroccan (*Reseda luteola* L.), wool dyeing, and antibacterial effectiveness. Fibers Polym. 24, 1051–1065. https://doi.org/10.1007/s12221-023-00019-9.

Ratto, D., Ferrari, B., Roda, E., Brandalise, F., Siciliani, S., De Luca, F., Priori, E.C., Di Iorio, C., Cobelli, F., Veneroni, P., Bottone, M.G., Rossi, P., 2020. Squaring the circle: a new study of inward and outward-rectifying potassium currents in U251 GBM cells. Cell. Mol. Neurobiol. 40, 813–828. https://doi.org/10.1007/s10571-019-00776-3.

Ruggeri, M., Bianchi, E., Rossi, S., Boselli, C., Icaro Cornaglia, A., Malavasi, L., Carzino, R., Suarato, G., Sánchez-Espejo, R., Athanassiou, A., Viseras, C., Ferrari, F., Sandri, G., 2022a. Maltodextrin-amino acids electrospun scaffolds cross-linked with Maillard-type reaction for skin tissue engineering. Biomater. Adv. 133. https://doi.org/10.1016/j.msec.2021.112593.

Ruggeri, M., Vigani, B., Boselli, C., Icaro Cornaglia, A., Colombo, D., Sànchez-Espejo, R., Del Favero, E., Mandras, N., Roana, J., Cavallo, L., Cantù, L., Viseras, C., Rossi, S., Sandri, G., 2022b. Smart nano-in-microparticles to tackle bacterial infections in skin tissue engineering. Mater. Today Bio 16. https://doi.org/10.1016/j.mtbio.2022.100418.

Ruggeri, M., Miele, D., Contardi, M., Vigani, B., Boselli, C., Icaro Cornaglia, A., Rossi, S., Suarato, G., Athanassiou, A., Sandri, G., 2023. Mycelium-based biomaterials as smart devices for skin wound healing. Front. Bioeng. Biotechnol. 11. https://doi.org/10.3389/fbioe.2023.1225722.

Russo, E., Spallarossa, A., Comite, A., Pagliero, M., Guida, P., Belotti, V., Caviglia, D., Schito, A.M., 2022. Valorization and potential antimicrobial use of olive mill wastewater (OMW) from Italian olive oil production. Antioxidants 11. https://doi.org/10.3390/antiox11050903.

Sciubba, F., Chronopoulou, L., Pizzichini, D., Lionetti, V., Fontana, C., Aromolo, R., Socciarelli, S., Gambelli, L., Bartolacci, B., Finotti, E., Benedetti, A., Miccheli, A., Neri, U., Palocci, C., Bellincampi, D., 2020. Olive mill wastes: a source of bioactive molecules for plant growth and protection against pathogens. Biology (Basel) 9, 1–20. https://doi.org/10.3390/biology9120450.

Shabir, S., Ilyas, N., Saeed, M., Bibi, F., Sayyed, R.Z., Almalki, W.H., 2023. Treatment technologies for olive mill wastewater with impacts on plants. Environ. Res. 216. https://doi.org/10.1016/j.envres.2022.114399.

Tagliabue, M., Tonziello, J., Bottino, A., Capannelli, G., Comite, A., Pagliero, M., Boero, F., Cattaneo, C., 2021. Laboratory scale evaluation of fertiliser factory wastewater treatment through membrane distillation and reverse osmosis. Membranes (Basel) 11. https://doi.org/10.3390/membranes11080610.

Tagliaferri, C., Davicco, M.J., Lebecque, P., Georgé, S., Amiot, M.J., Mercier, S., Dhaussy, A., Huertas, A., Walrand, S., Wittrant, Y., Coxam, V., 2014. Olive oil and vitamin D synergistically prevent bone loss in mice. PLoS One 9. https://doi.org/10.1371/journal.pone.0115817.

Tortosa, G., Alburquerque, J.A., Ait-Baddi, G., Cegarra, J., 2012. The production of commercial organic amendments and fertilisers by composting of two-phase olive mill waste (“alperujo”). J. Clean. Prod. 26, 48–55. https://doi.org/10.1016/j.jclepro.2011.12.008.

Verma, S., Singh, A., Kumari, A., Tyagi, C., Goyal, S., Jamal, S., Grover, A., 2017. Natural polyphenolic inhibitors against the antiapoptotic BCL-2. J. Recept. Signal Transduct. 37, 391–400. https://doi.org/10.1080/10799893.2017.1298129.

Yang, E.J., Yim, E.Y., Song, G., Kim, G.O., Hyun, C.G., 2009. Inhibition of nitric oxide production in lipopolysaccharide-activated RAW 264.7 macrophages by Jeju plant extracts. Interdiscip. Toxicol. 2, 245–249. https://doi.org/10.2478/v10102-009-0022-2.

Zubair, H., Bhardwaj, A., Ahmad, A., Srivastava, S.K., Khan, M.A., Patel, G.K., Singh, S., Singh, A.P., 2017. Hydroxytyrosol induces apoptosis and cell cycle arrest and suppresses multiple oncogenic signaling pathways in prostate cancer cells. Nutr. Cancer 69, 932–942. https://doi.org/10.1080/01635581.2017.1339818.